

Evolution of tin oxide (SnO₂) nanostructures synthesized by hydrothermal method

AJAY PRATAP SINGH GAHLOT (✉ apsgahlot@db.du.ac.in)

DESHBANDHU COLLEGE UNIVERSITY OF DELHI <https://orcid.org/0000-0002-9662-6969>

Rupali Pandey

AND college

Sandeep Singhania

AND College

Arijit choudhary

AND College

Amit Garg

AND College

Prof.Mridula Gupta (✉ mridula@south.du.ac.in)

Department of Electronic Sciences University of Delhi

Research Article

Keywords: Tin Oxide, nanostructures, sensing application

Posted Date: November 23rd, 2021

DOI: <https://doi.org/10.21203/rs.3.rs-1097943/v1>

License: © ⓘ This work is licensed under a Creative Commons Attribution 4.0 International License.

[Read Full License](#)

Abstract

Tin oxide (SnO_2), a versatile metal oxide due to its wide range of applications and its nature as an amphoteric oxide, has attracted researchers globally for many decades. Hydrothermal synthesis of wide band gap oxides with controllable nano shape and size is of primary attraction leading to myriad areas of applications such as electrodes in Lithium-ion batteries, gas sensing, photo-catalyst etc. to name a few. In this work, we have synthesized different types of nanostructures of Tin oxide through low temperature (180°C) Hydrothermal process by varying the concentration of its precursor solution ($\text{SnCl}_4 \cdot 5\text{H}_2\text{O}$) from 0.0625M to 0.25M. The characterization of as-synthesized SnO_2 done using UV-Vis spectroscopy, Scanning Electron Microscopy (SEM), Energy Dispersive X ray (EDX) and X-Ray Diffraction (XRD) confirm synthesis of tin oxide and formation of various nanostructures as a function of concentration of the precursor solution. The evolution of various shapes of nanostructures has been discussed in light of existing theories.

1. Introduction

Science and technological developments have led to various areas of applications of nano-materials and metal oxide semiconductor nanostructures. They have been studied for their vast range of applications such as photo-catalyst [1], Lithium-ion batteries [2], gas sensors [3,4] and various other industrial applications. Many semiconductor metal oxides such as ZnO , TiO_2 , WO_3 , have been widely investigated for these applications [5-11]. Thus, many attempts to prepare multi-morphology materials, namely, TiO_2 nano-rods [5] and nano-tubes [6], ZnO nano-rods [7] and nano-flowers [8], SnO_2 nano-rods [9] and nano-flowers [10-11] have been carried out by various methods. Amongst the various oxides, tin oxide (SnO_2) is of deep interest and have been investigated extensively for its unique properties. Tin oxide is an important n-type semiconductor with a wide band gap ($E_g = 3.6 \text{ eV}$), a large exciton binding energy (130 meV) and a high electron mobility ($100\text{-}200 \text{ cm}^2 \text{ V}^{-1} \text{ S}^{-1}$) [12]. SnO_2 is widely used in gas sensing [13-14]. In recent past, attention has been paid to SnO_2 nano-structures, in particular their hierarchical morphology due to their interesting physical and chemical properties. Numerous studies on tin oxide shows that we can tune the experimental parameters like solvent, pH, concentration, temperature, surfactant and time [15-18] to influence the morphology and structure of the final product. The crystal growth through a solution route can be controlled by the preparation conditions such as the introduction of additives, the solvent, precursor concentration, reaction temperature etc. It is well known that many experimental parameters such as the solvent, the solution pH, the OH^- concentration have a profound influence on the morphology of SnO_2 architectures. Many earlier studies were successful in preparing different morphologies of SnO_2 and in inducing characteristics related to these morphologies like Wang et.al [4,19] study on the synthesis and gas sensing of SnO_2 nano-rods and hollow micro-spheres, Yang et.al [20] study on self-assembled 3D flower-shaped SnO_2 nanostructure. Supothina et al. [16] reported the synthesis of SnO_2 nanorod clusters via hydrothermal route using different concentrations of precursor, $\text{Na}_2 \text{SnO}_3 \cdot 3\text{H}_2\text{O}$ and NaOH at 200°C for 48 h. Furthermore, a few studies report on the

synthesis of SnO₂ nanostructures using surfactants. Cao et al. [21] produced SnO₂ nano cubes and nanospheres using sodium dodecyl sulphate (SDS) as a surfactant via hydrothermal route at a temperature of 180 °C. But the usage of surfactants can cause environmental risks, especially to aquatic species. In another study, Matin et al. [22] successfully prepared SnO₂ nanoparticles without the use of any alkaline solution and template; however, the samples required further calcination at an elevated temperature of 350 °C following the hydrothermal process at 130 °C. Most of these studies are concerned with the synthesis SnO₂ nano-material in discrete morphologies by different methods. In this work, we have synthesized SnO₂ nano -spheres, nano-rods and nano-flowers by adjusting the precursor concentration via a simple hydrothermal route at a temperature of 180 °C using a mixture of water and ethanol as a solvent. This method does not need any surfactant, template or calcination to control the shape and the size of particles. In contrast, a concentrated sodium hydroxide solution was used to control the degree of hydrolysis during the synthesis of SnO₂ nanostructures. The effect of precursor concentration on morphology of SnO₂ is investigated and the evolution of various nanostructures of Tin oxide is studied and explained.

2. Experimental

Stannic chloride pentahydrate/tin (IV) chloride pentahydrate- SnCl₄.5H₂O (98%) was purchased from Himedia Laboratories Pvt. Ltd. Ethanol (99.9% with UN No.:1170). All chemical reagents were used as received without further purification. Synthesis process involves five different samples with different concentration of precursors. 1.753g of stannic chloride pentahydrate (SnCl₄.5H₂O (98%)) was dissolved into a solution of 40ml of distilled water and 40ml of ethanol and stirred for 15 mins at moderate speed, with drop-by-drop wise addition of 10ml solution of sodium hydroxide (NaOH- 6M) and ethanol (5ml each) to form 0.0625M solution. Afterwards, the obtained final mixture was transferred into Teflon mediated stainless steel autoclave of 100 ml capacity and hydrothermally treated at 180°C for 24 hours inside the muffle furnace. The obtained white precipitate from the autoclave was washed with ethanol and distilled water 4-5 times and then dried at 100°C for 2 hours.

The other two samples of different molarities were obtained by the same process by varying the concentration of precursor to get 0.167M and 0.25M solutions.

3. Results And Discussions

Optical characterization of the as-synthesized as well as hydrothermally processed samples has been done using UV-Vis spectroscopy. Morphology, size distribution and composition of the hydrothermally processed samples is determined using SEM and EDAX Analysis. Phase structure and phase purity of the as-synthesized nano- structures is determined using XRD. Some of the results obtained for these characterizations are discussed as under:

3.1 UV-Vis Measurements

The UV-Vis Spectrophotometry was done before and after hydrothermal synthesis process. Fig.(1a) and 1(b) shows the result obtained for the three different concentration of precursor solutions. As seen from fig.1(a), there is an upsurge in absorption from 190nm and the total absorption region extends up to 375nm for all the three as prepared samples. This is in contrast to the absorption region seen for hydrothermally processed samples as seen in fig.1(b). The absorption region is squeezed to a smaller region limited to around 275 nm with increase in absorptance peak value. This is indicative of the formation of different types of nanostructures as smaller particle size will absorb higher in shorter wavelength region.

3.2 XRD

The crystalline phase of hydrothermally synthesized SnO₂ samples were analyzed by XRD, and the typical XRD patterns for two compositions 0.0625M and 0.167M are shown in Fig. 2(a) and 2(b). Both the samples exhibits strong diffraction peaks corresponding to the planes (110),(101),(200),(211),(220),(310) and (112) at $2\theta = 27.28^\circ, 34.9^\circ, 39.66^\circ, 52.48^\circ, 55.78^\circ, 59.12^\circ$ and 66.42° . All these peaks can be indexed to tetragonal rutile structure of SnO₂ (JCPDS No.21-1250). We have further calculated the lattice parameter using the relation

$$\frac{1}{d^2} = \frac{4\sin^2\theta}{\lambda^2} = \frac{h^2 + k^2}{a^2} + \frac{l^2}{c^2} ; \lambda = 1.54 \text{ \AA}$$

The calculated values of lattice parameter are $a = 4.61 \text{ \AA}$ and $c = 3.09 \text{ \AA}$. The XRD pattern for the third composition 0.25M follows the similar trend. Further an increase in the peak intensity is observed with increase in precursor concentration. Also, FWHM decreases with increase in precursor concentration. It indicates increase in crystallite size with increase in precursor concentration.

3.3 EDAX Analysis

The EDAX Analysis of all the three Samples show prominent peaks indicating the presence of Sn and O elements in the samples as shown in figure.3(a) to 3(c). The weight percentage of Sn and O for the three samples is as shown in Table 1. It can be seen that the weight percentage of tin substantially decreases when the precursor concentration increases from 0.0625M to 0.167M. It is followed by a substantial increase in tin weight percentage when precursor concentration is further increased to 0.25M. The corresponding reverse trends is observed in the weight percent of the oxygen.

Table. 1 Weight percent of different elements in three samples

Element	Weight	Percentage	
concentration	0.0625M	0.167M	0.25M
Tin(Sn)	46.44	16.28	57.31
Oxygen(O)	53.56	83.72	42.69

3.4 SEM Analysis

The SEM images of the three samples with different concentrations of precursor solution is shown in fig.4(a) to 4(d). Fig.4(a) shows the SEM morphology of hydrothermally processed SnO₂ sample with precursor concentration of 0.0625M. The presence of numerous numbers of nanospheres can be easily seen. The formation of nanorods can be seen in fig.4(b). The length of the nanorods is of the order between 800-900 nm with an average diameter of around 400 nm. Fig.4(c) and 4(d) show the evolution of flower like nanostructure morphology. On close examination of fig.4(d), it can be clearly seen that the flower like morphology as the result of well-arranged nanorods. As seen in the XRD results, the crystalline behavior is enhanced with increase in precursor concentration with a corresponding increase in the crystallite size.

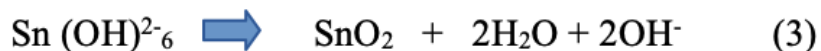
3.5 The SnO₂ nanostructures formation mechanism

Based on the obtained results, we propose a possible formation mechanism for SnO₂ nano-particles: SnO₂ nanoparticles are formed in two steps, namely dissolution and nucleation. At the early stage of the procedure, the precursor is dissolved in solvent and produced tin ions, Sn⁴⁺. When the concentrated NaOH is partly added into the solution, a white slurry was observed, showing the formation of Sn(OH)₄ (Eq. (1)). But then, as the pH reached pH 13, the white precipitate (Sn(OH)₄) dissolved immediately by reacting with abundant hydroxide ions and a transparent solution, Sn(OH)₆²⁻

was formed (Eq. (2)).



On the other hand, in the hydrothermal treatment as the concentration of Sn(OH)₆²⁻ complex increases with time, it eventually reaches a critical concentration where SnO₂ nuclei are formed spontaneously through the condensation reaction. (Eq. (3) [18].



The ratio of Sn⁺//OH⁻ plays an important role in the evolution of various nanostructures like nanospheres, nanorods and nanoflowers as elucidated by EDAX results. Nucleation leads to the formation of

nanospheres which is followed by crystal growth leading to formation of nanorods and then agglomeration in form of nanoflowers occurs with precursor concentration[23].

4. Conclusion

Synthesis of various nanostructures of SnO₂ like nanosphere, nanorods and nanoflowers have been experimentally performed by a simple hydrothermal route. The morphologies and shapes of the nanostructures found to be tuned by varying the concentrations of precursor solutions. A possible formation process and growth mechanism for such synthesized SnO₂ nanostructures have been studied. The effect of precursor concentration on morphology of SnO₂ is investigated and the evolution of various nanostructures of Tin oxide is studied and explained.

Declarations

Competing interests: The authors declare no competing interests.

Acknowledgement

Authors duly acknowledge the AIRF, JNU and CIF, DU facilities for various characterizations reported in this work. We are grateful to the Principal, Deshbandhu College and Principal, Acharya Narendra Dev College, University of Delhi for their support and infrastructure in carrying out of the experimental work.

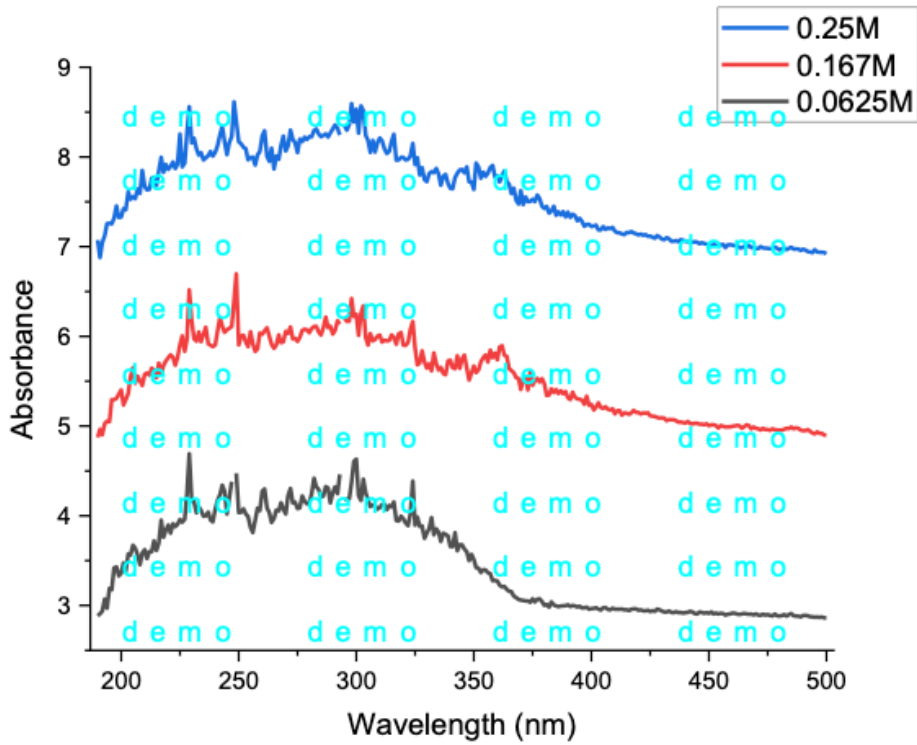
References

1. Tien HN, Luan VH, Hoa LT, Khoa NT, Hahn SH, Chung JS, et al. One-pot synthesis of a reduced graphene oxide-zinc oxide sphere composite and its use as a visible light photocatalyst. *Chem Eng J*. 2013 Aug 1;229:126–33.
2. Liu R, Li N, Li D, Xia G, Zhu Y, Yu S, et al. Template-free synthesis of SnO₂ hollow microspheres as anode material for lithium-ion battery. *Mater Lett [Internet]*. 2012;73:1–3. Available from: <http://dx.doi.org/10.1016/j.matlet.2011.12.035>
3. Hua Z, Tian C, Huang D, Yuan W, Zhang C, Tian X, et al. Power-law response of metal oxide semiconductor gas sensors to oxygen in presence of reducing gases. *Sensors Actuators, B Chem*. 2018 Aug 15;267:510–8.
4. Wang D, Chu X, Gong M. Gas-sensing properties of sensors based on single-crystalline SnO₂ nanorods prepared by a simple molten-salt method. *Sensors Actuators, B Chem*. 2006 Sep 12;117(1):183–7.

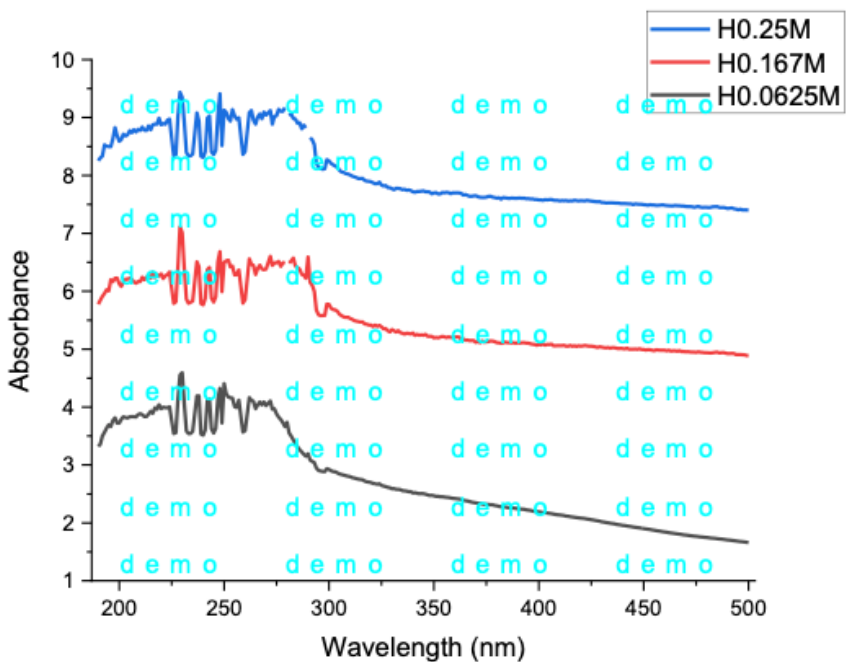
5. Li Y, Guo M, Zhang M, Wang X. Hydrothermal synthesis and characterization of TiO₂ nanorod arrays on glass substrates. *Mater Res Bull.* 2009;44(6):1232–7.
6. Song YY, Schmuki P. Modulated TiO₂ nanotube stacks and their use in interference sensors. *Electrochem Commun* [Internet]. 2010;12(4):579–82. Available from: <http://dx.doi.org/10.1016/j.elecom.2010.02.004>
7. Tao Y, Fu M, Zhao A, He D, Wang Y. The effect of seed layer on morphology of ZnO nanorod arrays grown by hydrothermal method. *J Alloys Compd.* 2010;489(1):99–102.
8. Feng L, Liu A, Liu M, Ma Y, Wei J, Man B. Synthesis, characterization and optical properties of flower-like ZnO nanorods by non-catalytic thermal evaporation. *J Alloys Compd.* 2010;492(1–2):427–32.
9. Shi S, Liu Y, Chen Y, Zhang J, Wang Y, Wang T. Ultrahigh ethanol response of SnO₂ nanorods at low working temperature arising from La₂O₃ loading. *Sensors Actuators, B Chem.* 2009;140(2):426–31.
10. Xu J, Wang D, Qin L, Yu W, Pan Q. SnO₂ nanorods and hollow spheres: Controlled synthesis and gas sensing properties. *Sensors Actuators, B Chem.* 2009 Apr 2;137(2):490–5.
11. Zhang H, Zeng W, Li Y, Miao B, Chen W. Synthesis of SnO₂ flower-like architectures by varying the hydrothermal reaction time. *J Mater Sci Mater Electron.* 2014;25(9):3674–9.
12. Diebold U. The surface science of titanium dioxide. *Surf Sci Rep* [Internet]. 2002;48(1):53–229. Available from: <http://linkinghub.elsevier.com/retrieve/pii/S0167572902001000>
13. Vuong DD, Sakai G, Shimano K, Yamazoe N. Hydrogen sulfide gas sensing properties of thin films derived from SnO₂ sols different in grain size. *Sensors Actuators, B Chem.* 2005;105(2):437–42.
14. Szuber J, Uljanow J, Karczewska-Buczek T, Jakubik W, Waczyński K, Kwoka M, et al. On the correlation between morphology and gas sensing properties of RGTO SnO₂ thin films. *Thin Solid Films.* 2005;490(1):54–8.
15. DEMAZEAU GWEST AR (Author of introductory parts); EJ (Author of introductory parts). *Solvothermal processes: a route to the stabilization of new materials.* Journal of material chemistry. 1999.
16. Supothina S, Rattanakam R, Vichaphund S, Thavorniti P. Effect of synthesis condition on morphology and yield of hydrothermally grown SnO₂ nanorod clusters. *J Eur Ceram Soc* [Internet]. 2011 Nov [cited 2021 Mar 26];31(14):2453–8. Available from: <https://www.sciencedirect.com/science/article/pii/S0955221911000781>

17. Talebian N, Jafarinezhad F. Morphology-controlled synthesis of SnO₂ nanostructures using hydrothermal method and their photocatalytic applications. *Ceram Int.* 2013 Sep;39(7):8311–7.
18. Inderan V, Lim S, Teng S, Bastien, Samuel B, Nadi L, Hooi L. Synthesis and characterisations of SnO₂ nanorods via low temperature hydrothermal method. *Superlattices and Microstructures*, 2015;88;396-402.
19. Wang L, Wang S, Wang Y, Zhang H, Kang Y, Huang W. Synthesis of hierarchical SnO₂ nanostructures assembled with nanosheets and their improved gas sensing properties. *Sensors Actuators, B Chem* [Internet]. 2013;188:85–93. Available from: <http://dx.doi.org/10.1016/j.snb.2013.06.076>
20. Yang R, Gu Y, Li Y, Zheng J, Li X. Self-assembled 3-D flower-shaped SnO₂ nanostructures with improved electrochemical performance for lithium storage. *Acta Mater* [Internet]. 2010;58(3):866–74. Available from: <http://dx.doi.org/10.1016/j.actamat.2009.10.001>
21. S. Cao, W. Zeng, H. Zhang, Y. Li, Hydrothermal synthesis of SnO₂ nanocubes and nanospheres and their gas sensing properties, *J. Mater. Sci. Mater. Electron.* 26 (2015) 2871e2878.
22. B. Mehrabi Matin, Y. Mortazavi, A.A. Khodadadi, A. Abbasi, A. Anaraki Firooz, Alkaline-and template-free hydrothermal synthesis of stable SnO₂ nanoparticles and nanorods for CO and ethanol gas sensing, *Sens. Actuators B Chem.* 151 (2010) 140e145.
23. Vuong D.D et.al. Synthesis of SnO₂ microspheres, nanorods and nano-flower via simple hydrothermal route. *Physica E.* 2011;44(2011) 345-349.

Figures



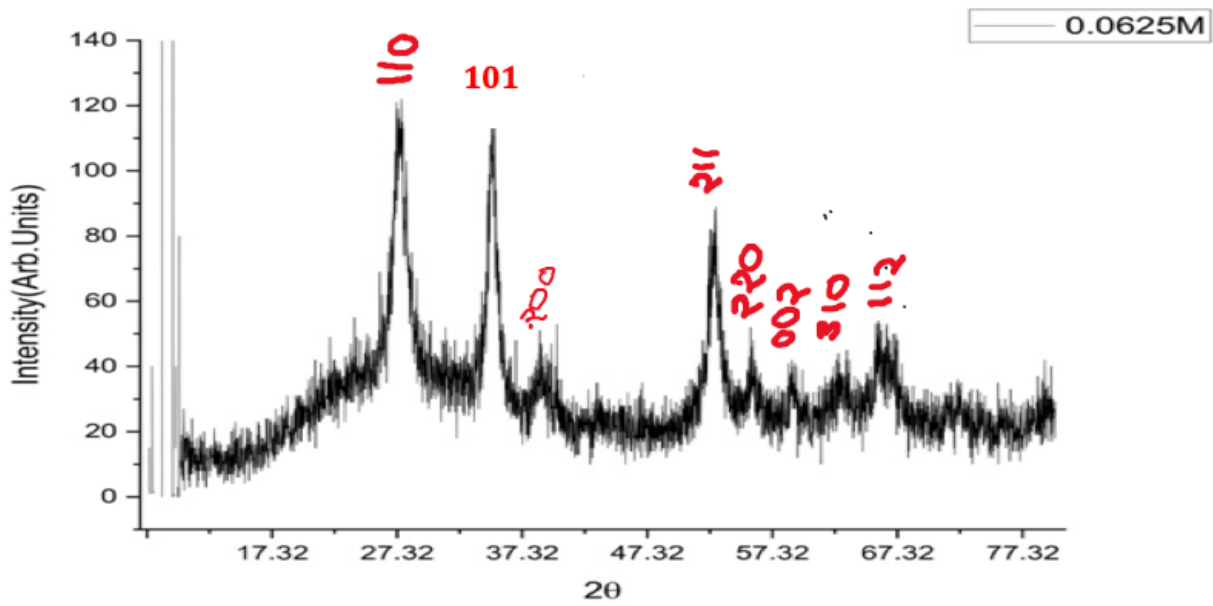
(a)



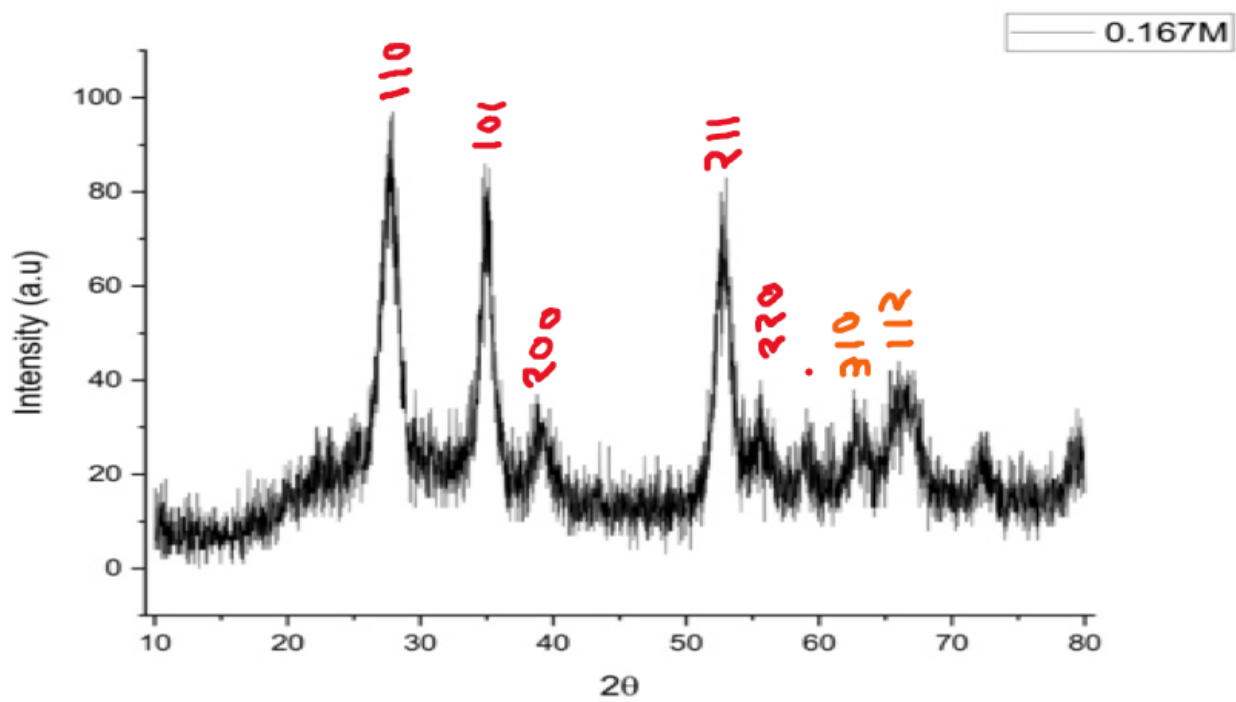
(b)

Figure 1

(a) UV-Vis Absorption of SnO₂ before Hydrothermal synthesis, (b) UV-Vis Absorption after hydrothermal synthesis of SnO₂.



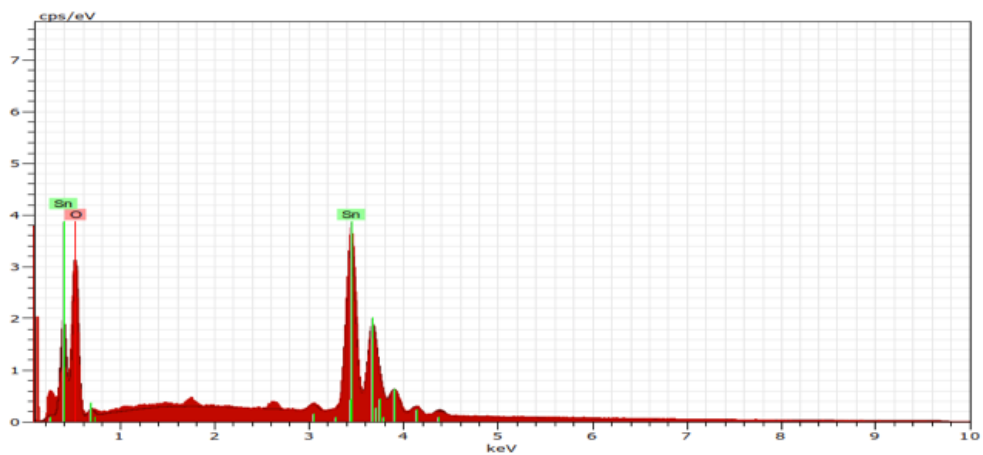
(a)



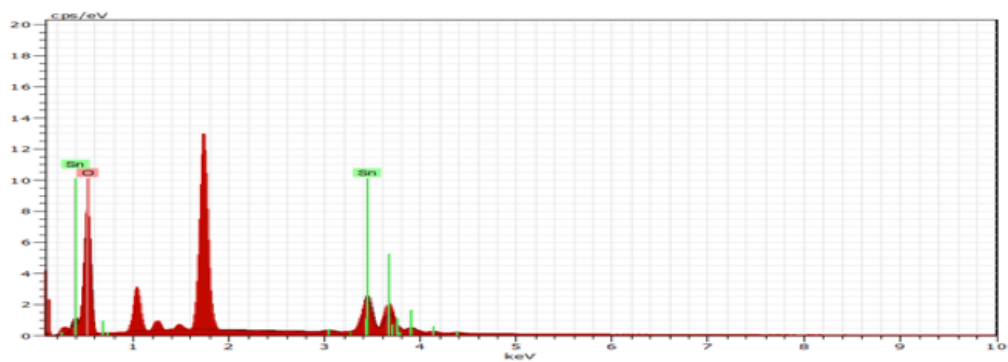
(b)

Figure 2

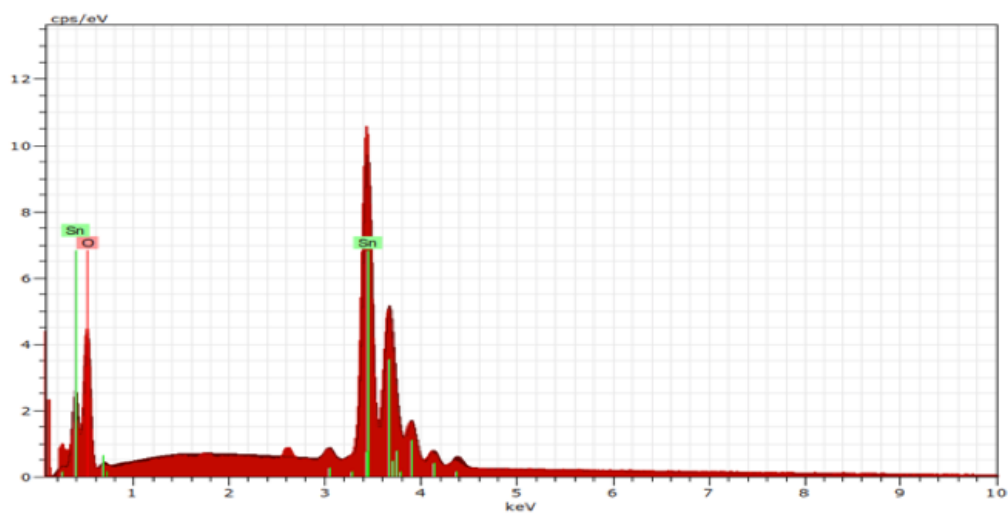
XRD of as prepared SnO₂ nanostructures with different concentration's of precursor (a) 0.0625M, (b) 0.167M.



(a)



(b)



(c)

Figure 3

EDAX Analysis of as prepared SnO₂ nanostructures (a) 0.0625M, (b) 0.167M, (c) 0.25M.

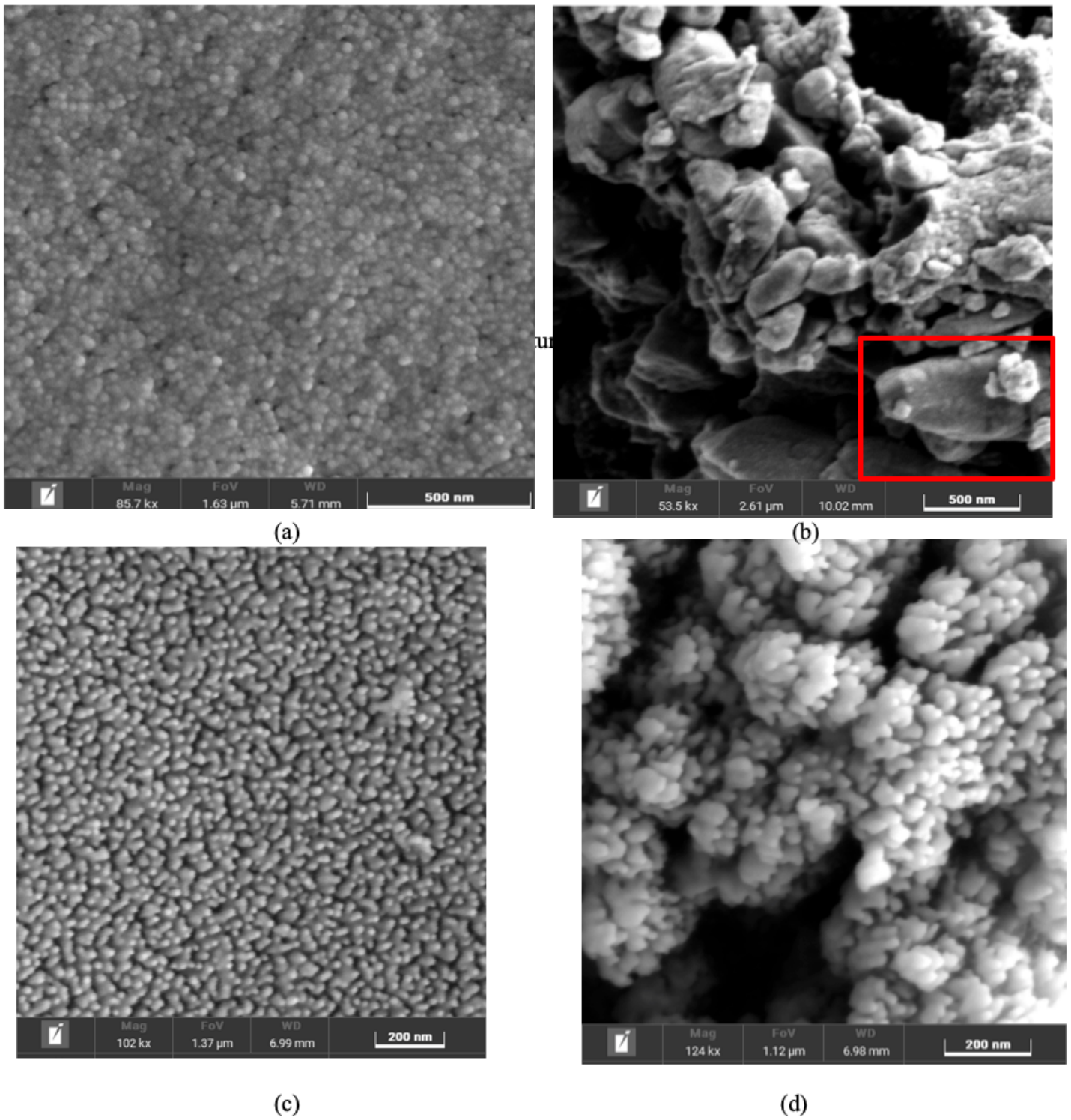


Figure 4

SEM Analysis of as prepared SnO₂ nanostructures (a) 0.0625M, (b) 0.167M, (c) and (d) 0.25M.

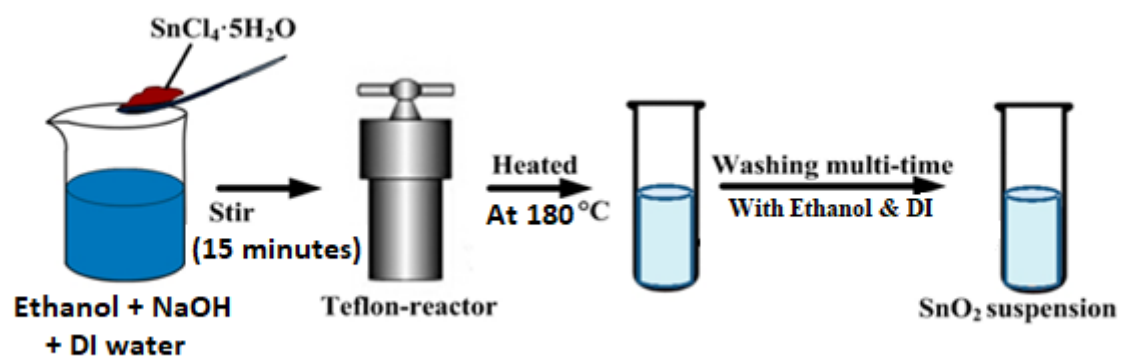


Figure 5

Experimental figure